# Dynamic Nonlinear Response of Cylindrical Shells to Asymmetric Pressure Loading

LAWRENCE J. MENTE*
*Kaman AviDyne, Burlington, Mass.*

**An analysis for the elastic nonlinear response of thin cylindrical shells to a time-dependent asymmetric pressure loading is developed through an energy formulation using Lagrangian equations of motion. These governing equations are established within the framework of large displacement shell theory and are solved through numerical methods for the temporal and spatial integrations. For selected shells the dynamic elastic response behavior, initial imperfection sensitivity and geometric nonlinearity effects are examined under asymmetric pressure loading. A definition of the threshold of elastic dynamic buckling is postulated based on the behavior of the peak circumferential flexural strain vs a specified loading parameter. Initial imperfections in several harmonics with amplitudes greater than one-tenth the shell's thickness can significantly increase (greater than 10%) the radial displacement response.**

## Nomenclature

| | |
|---|---|
| $a$ | = mean shell radius |
| $a_i, b_i$ | = integers |
| $E_x, E_\theta$ | = elastic moduli in the $x$ and $\theta$ directions |
| $G_{x\theta}$ | = shear modulus |
| $h$ | = shell thickness |
| $K$ | = $\kappa a$ |
| $l$ | = shell unsupported length |
| $L$ | = $l/\pi a$ |
| $m, n$ | = harmonic numbers in the axial and circumferential directions |
| $p(x, \theta, t)$ | = lateral time-dependent pressure loading |
| $p_r, p_i$ | = peak reflected and incident overpressures |
| $p_{mn}$ | = Fourier pressure coefficients |
| $R$ | = $a/h$ |
| $t$ | = time |
| $T$ | = kinetic energy |
| $u, v, w$ | = axial, circumferential and radial displacement components |
| $u_{mn}, v_{mn}, w_{mn}$ | = undetermined time-dependent displacement coefficients |
| $U, V, W$ | = $u/a, v/a, w/a$ |
| $\bar{w}$ | = initial radial imperfection |
| $\bar{W}$ | = $\bar{w}/a$ |
| $x, \theta, z$ | = cylindrical coordinates |
| $X$ | = dummy variable representing $U_{mn}$, $V_{mn}$, and $W_{mn}$ |
| $\alpha$ | = time decay constant |
| $\gamma$ | = $\pi x/l$ |
| $\Delta t$ | = time increment used in open-type integration method |
| $\delta_{mn}$ | = Fourier imperfection coefficients |
| $\varepsilon_{xx}, \varepsilon_{\theta\theta}, \varepsilon_{x\theta}$ | = membrane strains |
| $\kappa_{xx}, \kappa_{\theta\theta}, \kappa_{x\theta}$ | = change of curvature quantities |
| $\lambda$ | = 1 for $\gamma$ or 2 for $\theta$ integration |
| $\nu_x, \nu_\theta$ | = Poisson's ratios in the $x$ and $\theta$ directions |
| $\rho$ | = mass density |
| $\phi$ | = dummy variable representing $\gamma$ or $\theta$ |
| $\Psi$ | = strain energy |
| $\Omega$ | = potential energy of external loading |

*Subscripts*

| | |
|---|---|
| $e, 0$ | = $\beta$ even and odd |
| $x, \theta, \gamma$ | = partial spatial derivatives of displacement components |

*Superscripts*

| | |
|---|---|
| $e, 0$ | = $\beta$ even and odd |
| $f$ | = flexural strain |

Presented as Paper 72-357 at the AIAA/ASME/SAE 13th Structures, Structural Dynamics, and Materials Conference, San Antonio, Texas, April 10–12, 1972; received April 24, 1972; revision received December 18, 1972. This research was supported by the U.S. Army Ballistic Research Laboratories under Contract DA-18-001-AMC-1047(X), and U.S. Army Missile Command, Contract DAAH01-69-C-1809. The author wishes to thank J. M. Coco of Kaman AviDyne for her excellent programing as well as N. P. Hobbs and G. Zartarian for their significant contributions in formulating the numerical analysis.

Index category: Structural Dynamic Analysis.

* Senior Research Engineer.

## Introduction

REQUIREMENTS on many aerospace vehicles which consist of thin-walled shell sections necessitate the analysis of these shell sections to transient asymmetric pressure loading. The complete solution of this problem involves the connection of several computerized analyses which generate the loading parameters, the aerodynamics and the structural response of the critical shell sections. The complexities of such a complete code require that the structural response solutions be obtained within acceptable computer running times. The cylindrical or nearly cylindrical shell sections of these vehicles are buckling sensitive when subjected to lateral pressure loading, that is, elastic buckling usually occurs before plastic yielding of the material. To investigate the large displacement response of these shells, the analysis must be formulated within the framework of geometrical nonlinearities.

Comprehensive treatments for the nonlinear dynamic response of shells of revolution exist, for example, using the finite-difference[1] and finite-element[2] techniques. The modal-type solution formulated herein seeks to obtain a nonlinear response solution within acceptable computer time for just a cylindrical shell. When the number of harmonics required for an accurate solution are not excessive this objective is possible. This nonlinear analysis developed using large displacement shell theory is capable of predicting the dynamic response of a finite, simply supported, linear elastic cylindrical shell in the pre- and post-buckling regions. Numerical techniques are employed in the formulation which allow much flexibility in incorporating changes corresponding to different nonlinear shell theories and boundary conditions by minor programing alterations.

## Basic Theory

This analysis employs Hamilton's variational principle for conservative dynamic systems and a large displacement theory for shells to determine the elastic response of a finite thin-walled

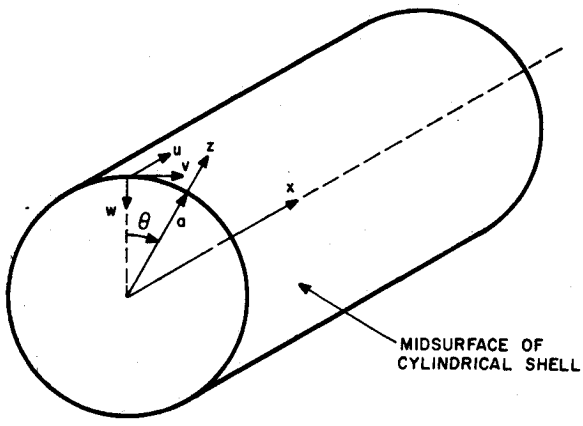


**Fig. 1 Shell coordinate system.**

cylinder. The cylindrical coordinates and positive directions of the displacement components are shown in Fig. 1. The displacement component functions for the midsurface of the shell are assumed in the form of truncated series of the product of undetermined time-dependent coefficients and assumed spatial functions which satisfy prescribed boundary conditions. The governing equations of motion for the cylindrical shells are formulated from Lagrangian equations in terms of the undetermined time-dependent coefficients and are given in the form

$$\frac{d}{dt}\left(\frac{\partial T}{\partial \dot{w}_{mn}}\right)+\frac{\partial \Psi}{\partial w_{mn}}+\frac{\partial \Omega}{\partial w_{mn}}=0 \qquad (m=1,2\ldots M),\quad (n=0,1,2\ldots N) \qquad (1)$$

where corresponding equations for $u_{mn}$ and $v_{mn}$ are also generated.

### Strain-Displacement Relations

The strain-displacement relations considered in this analysis are based on the assumptions: 1) strains are small compared with unity, 2) the thickness of the shell is small compared with the radius, and 3) the Kirchhoff-Love hypothesis that normals to the undeformed midsurface remain normal to the deformed midsurface and suffer no extension (neglects transverse shear and normal strains). The following set of strain-displacement relations is considered in the analysis where the midsurface membrane strain and change of curvature quantities are expressed in terms of the displacement components and their spatial derivatives

$$\begin{aligned}
\varepsilon_{xx} &= u_x+\frac{1}{2}[w_x{}^2+u_x{}^2+v_x{}^2] \\
\varepsilon_{\theta\theta} &= \frac{1}{a}v_\theta-\frac{1}{a}w+\frac{1}{2a^2}[(w_\theta+v)^2+(v_\theta-w)^2+u_\theta{}^2] \\
\varepsilon_{x\theta} &= v_x+\frac{1}{a}u_\theta+\frac{1}{a}w_x(w_\theta+v)+\frac{1}{a}v_x(v_\theta-w)+\frac{1}{a}u_\theta u_x
\end{aligned} \qquad (2)$$

$$\begin{aligned}
\kappa_{xx} &= w_{xx} \\
\kappa_{\theta\theta} &= \frac{1}{a^2}w_{\theta\theta}+\frac{1}{a^2}v_\theta+\frac{1}{a^2}(-w+v_\theta)+\frac{1}{a}u_x \\
\kappa_{x\theta} &= \frac{2}{a}w_{x\theta}+\frac{1}{a}v_x
\end{aligned} \qquad (3)$$

The entire set of terms of Eqs. (2) and (3) is attributed to Novozhilov,[3] except that Eq. (3) includes only the linear terms. The set of relations comprised of terms underlined by dashes is attributed to Sanders[4] while the set comprised of terms underlined by solid lines is attributed to Donnell.[5]

It is assumed that the initial imperfections of the cylindrical shell can adequately be included in the membrane strain-displacement relations by Donnell's representation.[5] This representation results in the addition of terms $w_x\bar{w}_x$ to $\varepsilon_{xx}$, $1/a^2 w_\theta \bar{w}_\theta$ to $\varepsilon_{\theta\theta}$ and $1/a(\bar{w}_x w_\theta+\bar{w}_\theta w_x)$ to $\varepsilon_{x\theta}$ in Eq. (2).

### Energy Formulation

The elastic strain energy of the cylindrical shell for an orthotropic material for which the geometric cylindrical coordinate axes and principal orthotropic directions are parallel is given[6] by

$$\begin{aligned}
\Psi=\int_0^l\int_0^{2\pi}\Bigg\{\frac{h}{2}\Bigg[&\frac{E_x}{1-\nu_x\nu_\theta}\varepsilon_{xx}{}^2+\frac{2\nu_x E_\theta}{1-\nu_x\nu_\theta}\varepsilon_{xx}\varepsilon_{\theta\theta}+ \\
&\frac{E_\theta}{1-\nu_x\nu_\theta}\varepsilon_{\theta\theta}{}^2+G_{x\theta}\varepsilon_{x\theta}{}^2\Bigg]+ \\
\frac{h^3}{24}\Bigg[&\frac{E_x}{1-\nu_x\nu_\theta}\kappa_{xx}{}^2+\frac{2\nu_x E_\theta}{1-\nu_x\nu_\theta}\kappa_{xx}\kappa_{\theta\theta}+ \\
&\frac{E_\theta}{1-\nu_x\nu_\theta}\kappa_{\theta\theta}{}^2+G_{x\theta}\kappa_{x\theta}{}^2\Bigg]\Bigg\}a\,dx\,d\theta
\end{aligned} \qquad (4)$$

The potential of the external pressure load $p(x,\theta,t)$ is defined as minus the work done by the external pressure. It is assumed that the pressure acts on the midsurface of the cylindrical shell. As the shell surface deforms, the elemental pressure force vector remains normal to the surface so that it changes direction during deformation. Furthermore, the magnitude of this force vector changes since the elemental surface area of the deformed shell changes. Thus, the work done by the external pressure over an arbitrary small time interval is defined as the product of the elemental pressure force and the displacement vector integrated over the cylindrical shell. The potential energy of the external pressure is expressed, with terms above the second order neglected, in the form

$$\Omega=a\int_0^l\int_0^{2\pi}p(x,\theta,t)\{-w+2w_\theta v/a+w^2/a+v^2/a+ w_x u-wu_x+w\bar{w}/a+v\bar{w}_\theta/a+u\bar{w}_x\}\,dx\,d\theta \qquad (5)$$

The kinetic energy of the cylindrical shell is given by

$$T=\frac{a\rho h}{2}\int_0^l\int_0^{2\pi}(\dot{u}^2+\dot{v}^2+\dot{w}^2)\,dx\,d\theta \qquad (6)$$

which neglects the rotary inertia contributions.

### Governing Equations of Motion

With the potential and kinetic energies defined either explicitly or implicitly in terms of displacement components and their derivatives, the governing Lagrangian equations of motion [Eq. (1)] are established using assumed midsurface displacement components which satisfy prescribed boundary conditions. The ends of the cylindrical shells are assumed to be simply supported in the sense that $w=v=w_{xx}=u_x=0$ are to be satisfied on the end boundaries at $x=0$ and $l$. Consistent with the above conditions, the displacement components are assumed in the form

$$\begin{aligned}
u &= \sum_{m=1}^{M}\sum_{n=0}^{N}u_{mn}(t)\cos n\theta\cos(m\pi x/l) \\
v &= \sum_{m=1}^{M}\sum_{n=0}^{N}v_{mn}(t)\sin n\theta\sin(m\pi x/l) \\
w &= \sum_{m=1}^{M}\sum_{n=0}^{N}w_{mn}(t)\cos n\theta\sin(m\pi x/l)
\end{aligned} \qquad (7)$$

For intermediate-length cylinders, whether the axial displacement constraint is free ($u_x=0$) or fixed ($u=0$) has a significant effect on the natural frequency and the critical static buckling pressure.[7,8] Hence, both of these boundary conditions are to be used to determine the significance of the axial displacement constraint on the nonlinear shell response. For $u=0$ at both

ends the $\cos m\pi x/l$ in the $u$ expression of Eq. (7) is replaced by $\sin 2m\pi x/l$. It should be noted that the frequency and static buckling parameters for intermediate-length cylinders are not significantly affected by whether the end rotational constraint is free ($w_{xx}=0$) or fixed ($w_x=0$).[7,8] The initial radial imperfections are represented in the Fourier expansion

$$\bar{w}=\sum_{m=1}^{M}\sum_{n=0}^{N}\delta_{mn}\cos n\theta\sin(m\pi x/l) \tag{8}$$

The consistent Fourier expansion of the lateral pressure loading is

$$p(x,\theta,t)=\sum_{m=1}^{M}\sum_{n=0}^{N}p_{mn}(t)\cos n\theta\sin(m\pi x/l) \tag{9}$$

The governing equations of motion for an orthotropic or isotropic elastic cylindrical shell are formulated through Eq. (1) by using Eqs. (4–6) for the energies and Eq. (7) for the displacement components and their derivatives. The normalized equation of motion for the radial displacement direction is given as follows

$$\begin{aligned}k\rho l^2\ddot{W}_{mn}+\int_0^{\pi}\int_0^{2\pi}\Bigg[&2L^2\Bigg\{\frac{E_\theta}{1-\nu_x\nu_\theta}\Bigg[\nu_x\left(\varepsilon_{\theta\theta}+\frac{1}{\nu_\theta}\varepsilon_{xx}\right)\frac{\partial\varepsilon_{xx}}{\partial W_{mn}}+\\&(\varepsilon_{\theta\theta}+\nu_x\varepsilon_{xx})\frac{\partial\varepsilon_{\theta\theta}}{\partial W_{mn}}\Bigg]+G_{x\theta}\varepsilon_{x\theta}\frac{\partial\varepsilon_{x\theta}}{\partial W_{mn}}\Bigg\}+\\&\frac{L^2}{6R^2}\Bigg\{\frac{E_\theta}{1-\nu_x\nu_\theta}\Bigg[(K_{\theta\theta}+\nu_xK_{xx})\frac{\partial K_{\theta\theta}}{\partial W_{mn}}+\\&\nu_x\left(K_{\theta\theta}+\frac{1}{\nu_\theta}K_{xx}\right)\frac{\partial K_{xx}}{\partial W_{mn}}\Bigg]+\\&G_{x\theta}K_{x\theta}\frac{\partial K_{x\theta}}{\partial W_{mn}}\Bigg\}+\frac{\partial\tilde{\Omega}}{\partial W_{mn}}\Bigg]d\gamma\,d\theta=0\end{aligned} \tag{10}$$

where $(m=1,2,3,\ldots M)$, $(n=0,1,2,\ldots N)$; $k=1$, for $n\neq 0$; $k=2$ for $n=0$, except for $V_{mn}$ equation where $k=0$ for $n=0$; $\varepsilon_{xx},\varepsilon_{\theta\theta},\varepsilon_{x\theta}$ and $K_{xx},K_{\theta\theta},K_{x\theta}$ are given by the normalized version of Eq. (2) and (3); the partial derivatives in Eq. (10) are readily obtained through Eqs. (2) and (3) and

$$\begin{aligned}\frac{\partial\tilde{\Omega}}{\partial W_{mn}}&=2L^2Rp\left[(-1+2W+\bar{W}-\frac{1}{L}U_\gamma)\frac{\partial W}{\partial W_{mn}}+\right.\\&\left.2V\frac{\partial W_\theta}{\partial W_{mn}}+\frac{1}{L}U\frac{\partial W_\gamma}{\partial W_{mn}}\right]\\\frac{\partial\tilde{\Omega}}{\partial V_{mn}}&=4L^2Rp[W_\theta+\tfrac{1}{2}\bar{W}_\theta+V]\frac{\partial V}{\partial V_{mn}}\\\frac{\partial\tilde{\Omega}}{\partial U_{mn}}&=2LRp\left[(W_\gamma+\bar{W}_\gamma)\frac{\partial U}{\partial U_{mn}}-W\frac{\partial U_\gamma}{\partial U_{mn}}\right]\end{aligned} \tag{11}$$

For the tangential and axial displacement directions the corresponding equations can be obtained from Eq. (10) by replacing $W_{mn}$ with $V_{mn}$ and $U_{mn}$, respectively.

## Numerical Analysis

The second-order differential equations given by Eq. (10) and corresponding equations for $V_{mn}$ and $U_{mn}$ are solved numerically. Two numerical methods were used for the temporal integration during the study. Initially, a Hamming's modified predictor-corrector method[9] for first-order differential equations was used by converting the second-order equations into sets of two first-order equations. Hamming's method is a stable fourth-order integration procedure which is able to choose and change the time increment to satisfy a prescribed accuracy criterion. Eventually, an open-type integration method was used to obtain a faster timewise solution of the second-order equations. This method is based on an open-type formula[10] given by

$$X_{i+1}=X_i+X_{i-2}-X_{i-3}+\left(\frac{\Delta t}{2}\right)^2(5\ddot{X}_i+2\ddot{X}_{i-1}+5\ddot{X}_{i-2}) \tag{12}$$

In comparing the solutions from the two methods, it was found that the latter method resulted in substantial reduction in computer time while still providing an adequate solution. For example, by using a time increment in the open-type method that corresponds to the maximum time increment which the Hamming's method eventually selects during the response, the maximum response quantities computed by the open-type method increased by less than 3% from the values computed by the Hamming's method. In this example, the open-type method provided an almost one-third reduction in computer time. Furthermore, by doubling this time increment in the open-type method, the response quantities only increased an additional 1 or 2% and the computer time was halved. Another 50% increase in the time increment used in the open-type method finally caused the solution to diverge.

Spatial integrations are performed in the $\gamma$ and $\theta$ variables during the stepwise time integration and are of the form

$$I_\lambda=\int_0^{\lambda\pi}(\cos a_1\phi\cos a_2\phi\ldots\cos a_\eta\phi)\times(\sin b_1\phi\sin b_2\phi\ldots\sin b_\beta\phi)\,d\phi \tag{13}$$

The integrations are to be effected numerically through the use of Gaussian quadrature formulas. To apply the appropriate quadrature formula, the integrand of Eq. (13) is cast into a polynomial form, $P_S(\cos\phi)$, of order $S$. Thus, it can be shown that the integrand is expressible in polynomial form as

$$\begin{aligned}&P_{(S_1+S_2-1)}(\cos\phi)\sin\phi, &&\text{for } \beta \text{ odd}\\&\tilde{P}_{(S_1+S_2)}(\cos\phi), &&\text{for } \beta \text{ even}\end{aligned}$$

where

$$S_1=\sum_{i=1}^{\eta}a_i \quad\text{and}\quad S_2=\sum_{i=1}^{\beta}b_i$$

Then for $\lambda=1$, through the variable change $\xi=\cos\gamma$, the integrals for $\beta$ odd and even are given, respectively, in the forms required by the Legendre-Gauss and Chebyshev-Gauss quadrature formulas,[10] so that

$$I_1{}^0=\sum_{k=1}^{\bar{M}}H_kP_{(S_1+S_2-1)}(\xi_k)+E_0 \tag{14}$$

$$I_1{}^e=\frac{\pi}{\bar{M}}\sum_{k=1}^{\bar{M}}\tilde{P}_{(S_1+S_2)}\left(\cos\frac{2k-1}{2\bar{M}}\pi\right)+E_e \tag{15}$$

where

$$H_k=2(1-\xi_k{}^2)/(\bar{M}+1)^2[P_{\bar{M}+1}(\xi_k)]^2$$

The $\xi_k$'s are the zeros of the Legendre polynomial $P_{\bar{M}}(\xi)$, $E_0$ and $E_e$ are the error terms and are proportional to $P^{(2\bar{M})}(\xi)$. Thus, if $2\bar{M}\geqq S_1+S_2$ for $\beta$ odd or $2M>S_1+S_2$ for $\beta$ even, the error is zero and the integration is exact. It is noted that

$$\gamma_k{}^0=\cos^{-1}(\xi_k)(\beta\,\text{odd}),\quad \gamma_k{}^e=\frac{2k-1}{2\bar{M}}\pi(\beta\,\text{even}) \tag{16}$$

For the $\theta$-integration, $\lambda=2$, for which it can be shown that $I_2{}^0=0$ and $I_2{}^e=2I_1{}^e$, previously derived formulas for the $\gamma$-integration hold true with $\gamma$, $\bar{M}$ and $k$ replaced by $\theta$, $\bar{N}$ and $j$ in Eqs. (15) and (16).

The integrand in Eq. (10), defined as $f(\gamma,\theta;t)$, is separated into parts for $\beta$ odd and even as $f_0(\gamma,\theta)$ and $f_e(\gamma,\theta)$, respectively. Then the spatial integrations to be performed at each time step are given by

$$\int_0^{\pi}\int_0^{2\pi}f_0(\gamma,\theta)\,d\gamma\,d\theta=\frac{2\pi}{\bar{N}}\sum_{k=1}^{\bar{M}}\sum_{j=1}^{\bar{N}}H_k\frac{f_0(\gamma_k{}^0,\theta_j)}{\sin\gamma_k{}^0}\quad(\beta\,\text{odd}) \tag{17}$$

$$\int_0^{\pi}\int_0^{2\pi}f_e(\gamma,\theta)\,d\gamma\,d\theta=\frac{2\pi^2}{\bar{M}\bar{N}}\sum_{k=1}^{\bar{M}}\sum_{j=1}^{\bar{N}}f_e(\gamma_k{}^e,\theta_j)\quad(\beta\,\text{even}) \tag{18}$$

where $\bar{M}$ and $\bar{N}$ can be chosen to give an exact integration.

## Numerical Results

This computerized analysis, called DEPICS, is exercised for two cylindrical shells subjected to an asymmetric pressure

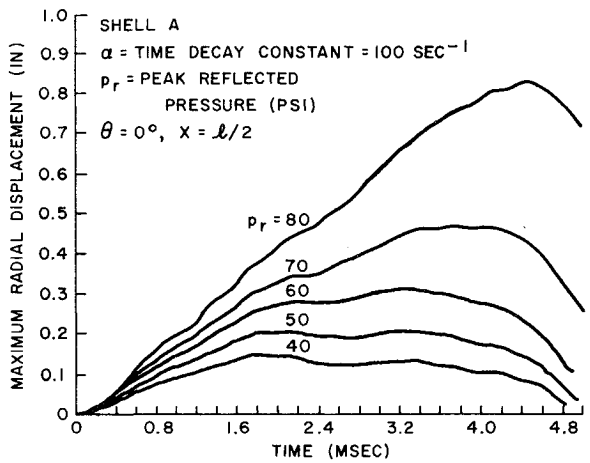


Fig. 2 Radial displacement time histories for shell A.

loading. The applications are selected to illustrate the dynamic nonlinear behavior of these buckling-sensitive shells, initial imperfection sensitivity and geometric nonlinearity effects. The two shells selected are an isotropic (Shell A) and an orthotropic (Shell B) shell section. The geometries and material properties for these two shells are given in Table 1.

The asymmetric pressure loading used for these applications is given by

$$p(x,\theta,t) = [(p_r - p_i)\cos^2\theta + p_i]\, e^{-\alpha t}\left(-\frac{\pi}{2} \leqq \theta \leqq \frac{\pi}{2}\right)$$
$$= p_i e^{-\alpha t} \qquad \left(\frac{\pi}{2} < \theta < \frac{3\pi}{2}\right) \tag{19}$$

The relationship between $p_r$ and $p_i$ is obtained from air blast results.[11] A time decay constant of 100 $sec^{-1}$ is used for the Shell A applications while 250 $sec^{-1}$ is used for the Shell B applications.

### Elastic Response Behavior

The response behavior is determined using Novozhilov's nonlinear strain-displacement relations for Shell A and B at various pressure levels. The solutions are determined using the Hamming's method and an exact spatial integration. Eleven circumferential harmonics ($n = 0$–10) are used in all applications.

Table 1 Shell section properties

| | Shell A | Shell B |
|---|---|---|
| $a$ (in.) | 11.8 | 12.55 |
| $l$ (in.) | 42.0 | 40.0 |
| $h$ (in.) | 0.2 | 0.267 |
| $E_\theta$ (psi) | $6 \times 10^6$ | $4.6 \times 10^6$ |
| $E_x$ (psi) | $6 \times 10^6$ | $3.24 \times 10^6$ |
| $G_{x\theta}$ (psi) | $2.59 \times 10^6$ | $1.2 \times 10^6$ |
| $\nu_\theta$ | 0.16 | 0.173 |
| $\nu_x$ | 0.16 | 0.122 |
| $\rho$ (lb-sec$^2$/in.$^4$) | $1.88 \times 10^{-4}$ | $2.74 \times 10^{-4}$ |

The number of axial harmonics required for sufficient accuracy varied from $m = 1$ to $m = 1, 3, 5$ as the peak reflected pressure increased. Figures 2 and 3 are time history plots of the maximum radial displacement at the midlength of the two shell sections for several values of the peak reflected overpressure, $p_r$. These figures show an apparent change in the character of the radial displacement time history with increasing load parameter $p_r$. This change in behavior corresponds to an increase in the time of peak response as the load parameter increases which can be attributed to a rapid increase in flexural response over membrane response within the shells. This transition in behavior occurs between $p_r$ of 40 and 50 psi for Shell A and $p_r$ of 85 and 100 psi for Shell B.

Typical strain time histories at $\theta = 0°$ on the inner and outer surfaces of Shell B are illustrated in Fig. 4 at $p_r = 125$ psi. It may be observed from the outer and inner surface strain time histories that at very early times the character of the deformation is primarily membrane while the flexural deformation becomes increasingly dominant with time in the circumferential direction and to a much lesser extent in the axial direction.

### Harmonic Content Evaluation

The number of harmonics used circumferentially and axially for a response calculation certainly has an influence on the accuracy of the solution. By employing 15 instead of 11 circumferential harmonics for the Shell A solution at $p_r = 70$ psi, it is found that the influence of the additional harmonics on the response is insignificant. The influence of the number of axial harmonics used for the solution of the displacement response of Shell B is illustrated in Fig. 5. These solutions were obtained using the open-type temporal integration method. It is

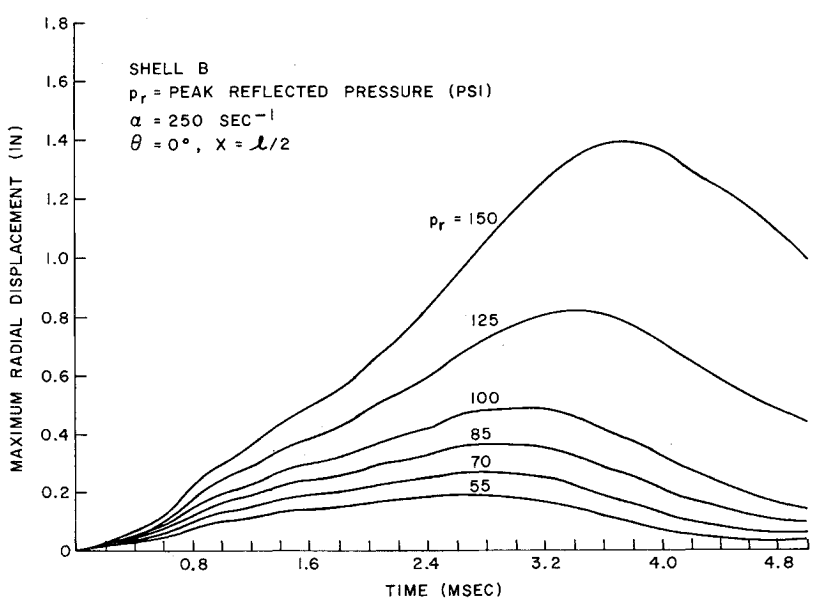


Fig. 3 Radial displacement time histories for shell B.

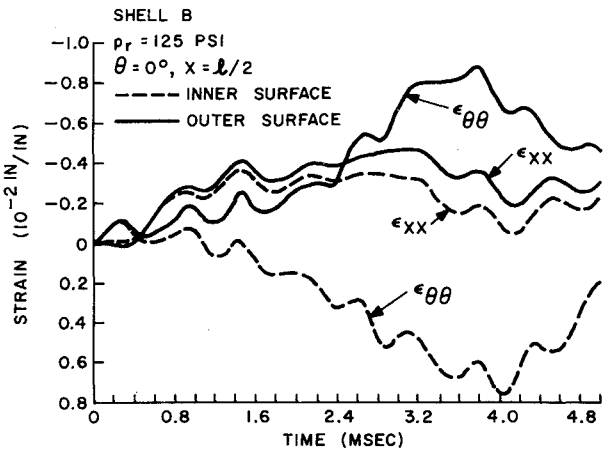


Fig. 4 Strain time histories.

found that as the peak radial displacement becomes large (greater than $2h$) more axial harmonics than $m = 1$ are needed for an accurate solution. For loads between $p_r = 100$ and 150 psi, the combination of axial harmonics $m = 1$ and 3 provides an adequate solution, since the $m = 1$, 3 and 5 solution practically converges for $p_r = 125$ psi and is close for $p_r = 150$ psi. The change in the displacement response when more harmonics are used is characterized by a larger peak amplitude and time of maximum response. The influence of axial harmonics on the strain responses is shown in Fig. 6 at the largest load ($p_r = 150$ psi) for the various combinations of harmonics $m = 1$, 3 and 5. The over-all strain response does not converge as well as the radial displacement response, but the peak amplitude of the circumferential and axial strains differ by only 5% and 1.2%, respectively, between the $m = 1$, 3 and $m = 1$, 3 and 5 solutions.

### Dynamic Buckling Determination

The buckling behavior, particularly the threshold of elastic buckling, of these two shells under asymmetric loading are examined through the response results obtained. In general, the threshold of dynamic elastic buckling may be defined as the initial occurrence of large increases in the peak displacement response for a small change in load amplitude. This dynamic buckling criterion is usually based on a plot of a peak displacement parameter vs a load amplitude parameter for the various response curves obtained. The peak radial displacement vs peak load parameter ($p_r$) plots are illustrated for Shell A and

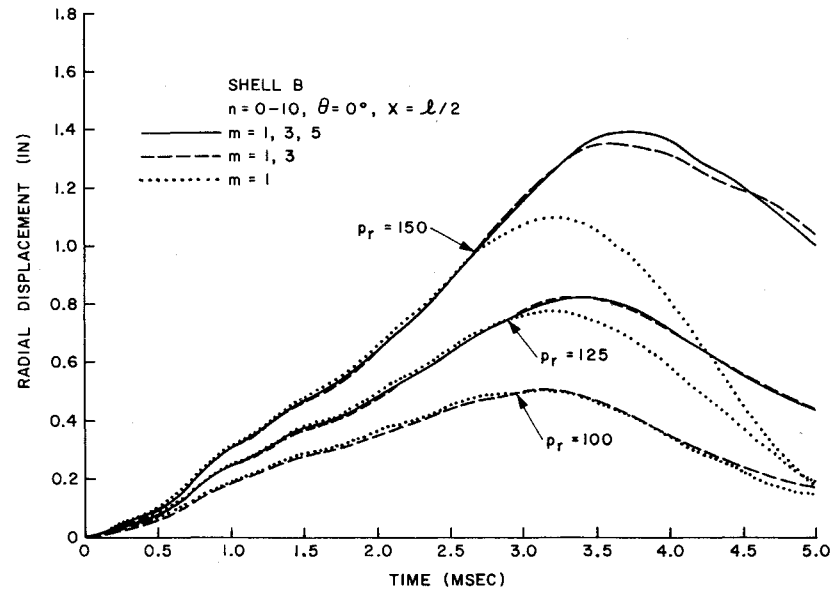


Fig. 5 Influence of axial harmonics on displacement response.

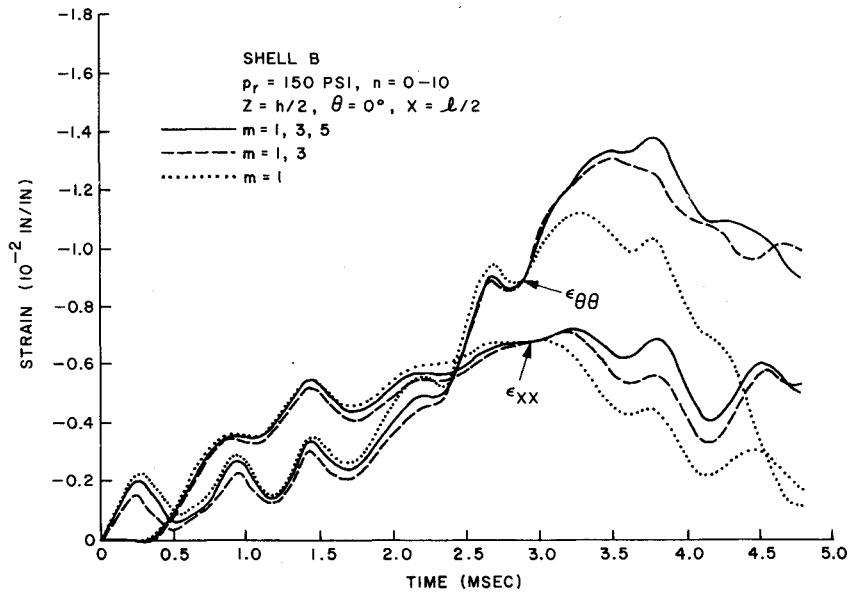


Fig. 6 Influence of axial harmonics on strain response.

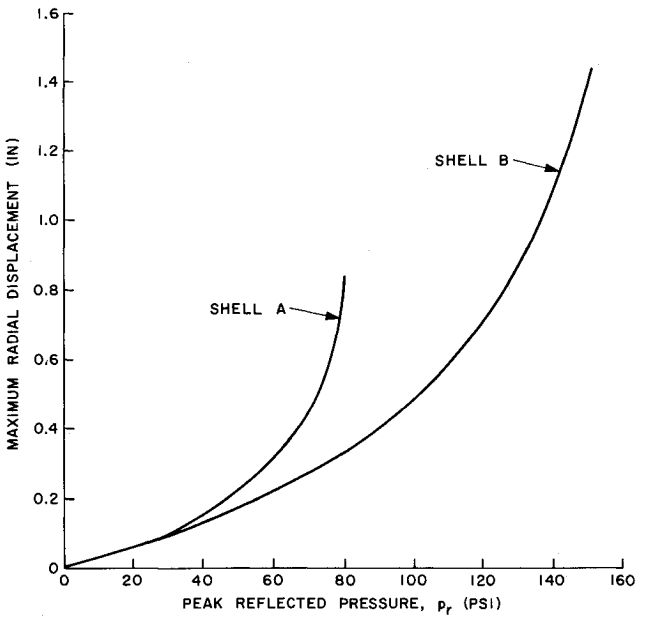


Fig. 7 Maximum radial displacement vs load parameter.

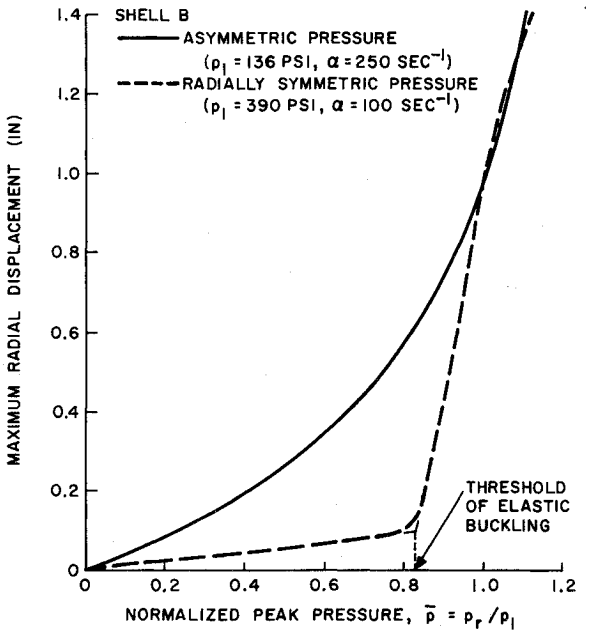


Fig. 9 Contrast between peak response from asymmetric and symmetric pressure loads.

B in Fig. 7. The plots do show a large region of loading over which the peak displacement amplitude is increasing more rapidly with a given load increment; but they do not exhibit a discontinuity region, characteristic of plots for axially loaded cylinders and uniformly loaded shallow spherical caps, which defines a loading value for the threshold of elastic buckling. Under the asymmetric loading on Shells A and B, the concentration of the pressure loading on the windward side forces the shell, even at low levels of loading, into a deformed shape that has characteristics similar to the buckled shape attained at higher loading levels; thus, the transition between the prebuckling and postbuckling displacement response is more gradual. This similarity in deformed shape is illustrated in Fig. 8 where the maximum normalized radial displacement profiles for Shell B are given for load levels less than 85 psi and greater than 100 psi.

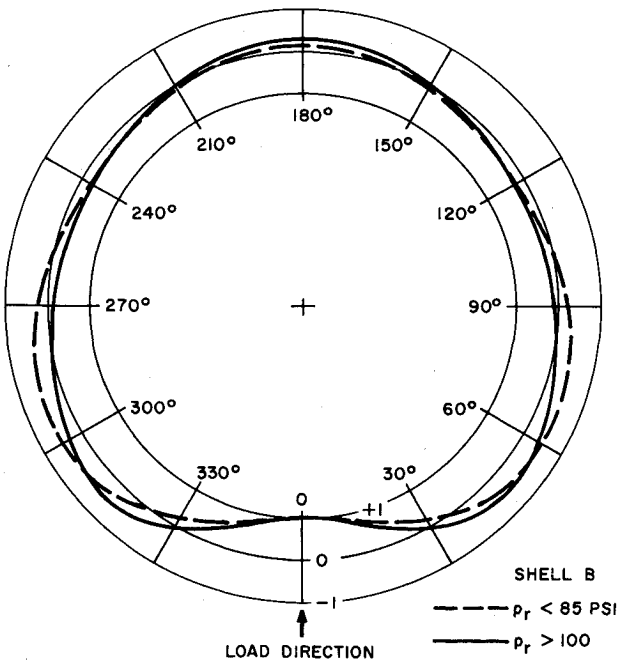


Fig. 8 Normalized radial displacement profile at time of maximum response for various loading regions.

For contrast, a peak response-load parameter plot for Shell B subjected to a radially symmetric pressure load ($\alpha = 100$ sec$^{-1}$) is illustrated in Fig. 9 with the plot for the asymmetric loading. The load parameter axis in Fig. 9 is normalized by the peak pressure required to produce a 1-in. peak radial displacement. For the symmetric load case, the shell is assumed to have a very slight initial radial imperfection in the third and sixth circumferential harmonics. In the prebuckling region of the symmetric load plot, the radial displacement response is dominated by the zeroth harmonic; however, in the buckling region the much different deformed shape is dominated by response in the sixth harmonic. Figure 9 shows that the shape of the symmetric load plot is very different from the asymmetric load plot and much more conducive for estimating the threshold of elastic buckling. It should be noted that if the geometric imperfections are increased the shape of the symmetric load plot would become similar to the other plot whose asymmetric loading represents a significant imperfection from a source other than shell geometry.

In the search for a definitive determination for the threshold of elastic buckling, a more sensitive response parameter is considered for these shells subjected to an asymmetric pressure loading. Since shell buckling is characterized by a large increase in the circumferential flexural response, a more sensitive response parameter is the peak circumferential flexure strain given by $\varepsilon_{\theta\theta}{}^f = [\varepsilon_{\theta\theta}(h/2) - \varepsilon_{\theta\theta}(-h/2)]/2$. Figure 10 illustrates the curves for the maximum circumferential flexure strain at $\theta = 0°$ vs loading parameter $p_r$ for both shells. The important behavior is the apparent inflection in each curve where the circumferential flexure strain increases more rapidly over a small region of the loading parameter. The loading parameters associated with the inflection points for Shell A and B are found to be $p_r = 45$ psi and 92 psi, respectively. These load parameter values correspond closely to the mean values of the aforementioned load parameter regions associated with a shift in the time of maximum response, an increase in the flexural behavior and a change in the deformed shape of the shell. For these shells, the threshold of elastic buckling is assumed to be defined approximately by the above inflection point loading parameters.

### Initial Imperfection Sensitivity

This sensitivity evaluation was performed for Shell B using 11 circumferential harmonics ($n = 0$–10) and just one axial

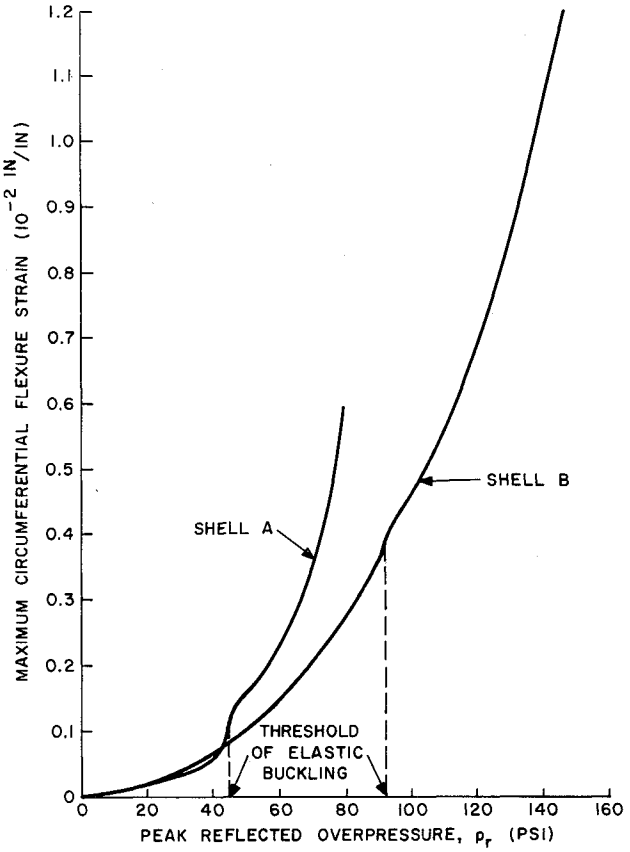


Fig. 10 Maximum circumferential flexure strain vs load parameter.

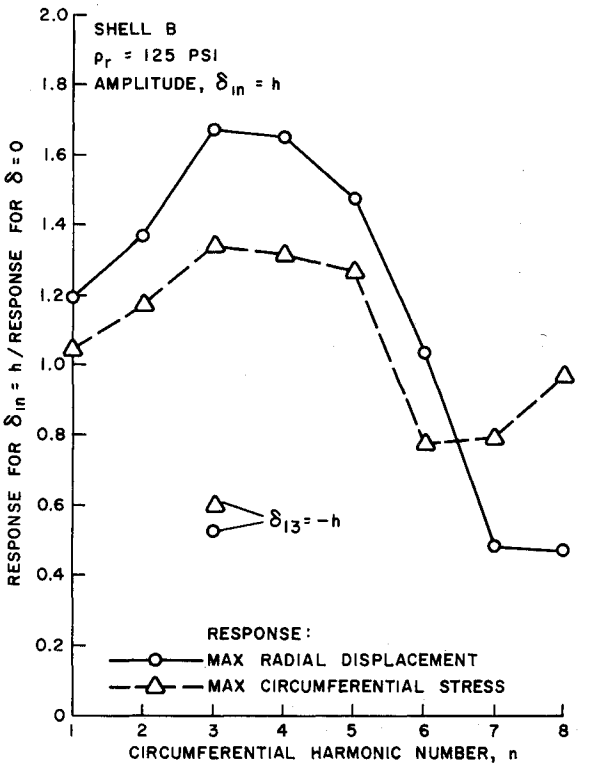


Fig. 12 Initial imperfection shape sensitivity.

harmonics ($m = 1$), since only trends were being investigated. In this evaluation only individual harmonics from Eq. (8) were used in the solutions for the initial imperfection of the cylinder. The changes in response produced by varying the amplitude and circumferential harmonic number ($n$) were examined at peak reflected pressures of 70 and 125 psi which correspond, respectively, to levels before and after the threshold of buckling. In Fig. 11 the imperfection amplitude normalized by the shell's thickness is plotted vs the maximum radial displacement response normalized with respect to the displacement value without imperfection ($\delta = 0$). This figure illustrates the initial imperfection amplitude sensitivity for the third circumferential harmonic for the two $p_r$ levels. It is apparent in Fig. 11 that initial imperfections at amplitudes greater than about one-tenth of the shell's thickness can significantly affect the shell response. Shell B is more sensitive to the initial imperfections at the peak reflected pressure level at 70 psi than at 125 psi. This observation seems to indicate that initial imperfections have a greater influence on response near the threshold of buckling than later in the postbuckling region.

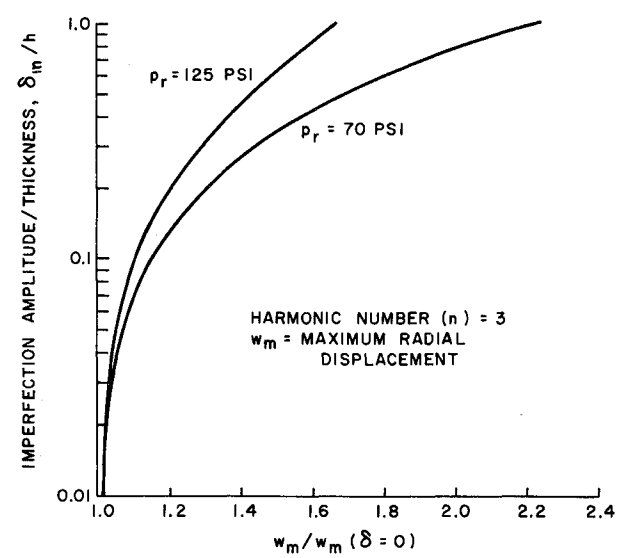


Fig. 11 Initial imperfection amplitude sensitivity.

The response sensitivity to the shape (or harmonic) of the initial imperfection for both displacement and stress is illustrated in Fig. 12. In this figure the maximum response for an imperfection amplitude equal to the shell's thickness normalized by the corresponding response for a perfect shell is plotted vs the circumferential harmonic number ($n$) for the $p_r = 125$ psi loading. Figure 12 shows that the shell response is most sensitive to the third harmonic, but several other harmonics, such as $n = 2, 4$, and 5 can also significantly affect the response. It can be seen that imperfection harmonics greater than six have a strengthening effect on the shell since the response produced is less than that of the perfect shell. It might be that these higher harmonic imperfections produce sort of a longitudinal corrugated stiffened shell. Figure 12 also shows that the displacement response is more sensitive to imperfections than the stress response. A substantial strengthening effect is also produced when the shell is oriented such that the initial imperfection at $\theta = 0°$ is outward instead of inward. This is indicated in Fig. 12 for the third harmonic with an amplitude of minus the shell's thickness.

### Response Evaluation of Various Geometric Nonlinearities

Since this evaluation is only to establish trends among the different theories, the response solutions are obtained using one axial harmonic ($m = 1$) to minimize computer time. The results from this investigation are tabulated in Table 2 where the maximum radial displacements and circumferential stresses predicted by the three shell theories indicated in Eqs. (2) and (3) are compared at various load levels defined by $p_r$. The time of maximum radial displacement is also given in the table as a characteristic of the time history of response. From Table 2 it

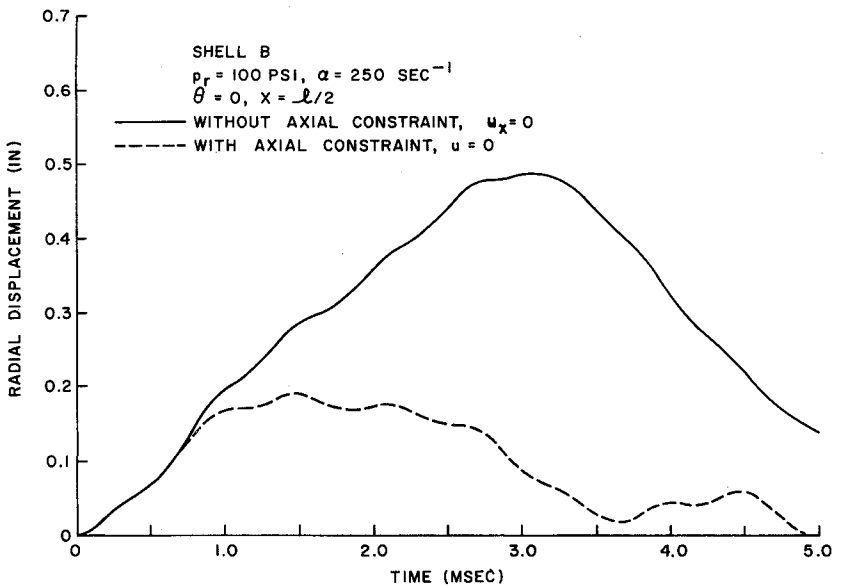


**Fig. 13 Effect of axial boundary constraints on radial displacement response.**

is seen that, for this particular shell and loading condition, the Donnell and Sanders theories give a reasonable solution for displacement response when compared to the more accurate Novozhilov theory over the range of pressure loads considered. The Sanders theory compared very closely (within 1%) while the Donnell theory predicted 4 or 5% higher response with a smaller time of maximum response. In comparing maximum circumferential stresses in Table 2 between the Sanders and Donnell theory predictions, it is seen that the Donnell theory predicts about 12% higher. Although the differences among the theories found in this application using Shell A are small, the results should not be extrapolated to other shells and loading conditions.

#### Axial Boundary Constraint Effects

Figure 13 illustrates for Shell B with $p_r = 100$ psi the significant difference between the maximum radial displacement responses with ($u = 0$) and without ($u_x = 0$) axial end boundary constraints. When the ends of the cylinder are fixed axially ($u = 0$), the peak radial displacement is reduced by 61% and occurs much earlier in the response. The peak circumferential and axial strains in this shell are reduced by 48% and 60%, respectively, for the $u = 0$ boundary condition.

## Conclusions

1) Acceptable computer running times are achieved with the DEPICS analysis. For example, on a CDC 6600 computer using the open-type integration method ($\Delta t = 10^{-5}$ sec), Shell B, 11 circumferential harmonics and an exact spatial integration, the computer times are 17 sec per msec of response for a $m = 1$ solution and 52 sec per msec of response for a $m = 1, 3$ solution.

2) For the selected shells the threshold of elastic buckling is assumed to be defined by the pressure parameters associated with the inflections in the plots of the maximum circumferential flexure strain vs the loading parameter.

3) An initial imperfection can significantly affect the shell response when the amplitude of the imperfection harmonic coefficient is greater than one-tenth the shell's thickness for any of several harmonics ($2 \leqq n \leqq 5$), provided the orientation of the harmonics relative to the load direction is optimum.

4) For the selected shells, the differences in the response quantities determined from the various nonlinear shell theories considered are small, but this result should not be extrapolated to other shells and loading conditions.

5) Whether the axial boundary constraint for the shell is free ($u_x = 0$) or fixed ($u = 0$) has a significant effect on the midlength response quantities.

**Table 2 Response comparison employing various nonlinear shell theories (Shell A—response at $\theta = 0°$, $x = l/2$)**

| Load parameter $p_r$, psi | Maximum radial displacement, in. | | | Max circum stress, psi | |
|---|---|---|---|---|---|
| | Donnell theory | Sanders theory | Novozhilov theory | Donnell theory | Sanders theory |
| 40 | 0.1557(1.80)[a] | ... | 0.1514(1.81) | ... | ... |
| 50 | 0.2186(3.30) | 0.2093(3.35) | 0.2093(3.45) | −16460 | −14300 |
| 60 | 0.3334(3.30) | 0.3145(3.35) | 0.3145(3.34) | −24023 | −21499 |
| 70 | 0.4755(3.30) | 0.4497(3.35) | 0.4498(3.35) | −33197 | −29641 |
| 80 | ... | 0.6042(3.35) | 0.6037(3.34) | ... | ... |
| 100 | 0.9611(2.75) | 0.9224(3.05) | 0.9206(3.03) | −62842 | −55531 |

[a] Indicates the time of maximum displacement in msec.

## References

[1] Morino, L., Leech, J. W., and Witmer, E. A., "An Improved Numerical Calculation Technique for Large Elastic-Plastic Transient Deformations of Thin Shells," *Journal of Applied Mechanics*, June 1971, pp. 423–436.

[2] Stricklin, J. A. et al., "Nonlinear Dynamic Analysis of Shells of Revolution by Matrix Displacement Method," *AIAA Journal*, Vol. 9, No. 4, April 1971, pp. 629–636.

[3] Novozhilov, V. V., *Foundations of the Nonlinear Theory of Elasticity*, Graylock Press, Rochester, N.Y., 1953.

[4] Sanders, J. L., Jr., "Nonlinear Theories for Thin Shells," *Quarterly of Applied Mechanics*, Vol. XXI, No. 1, 1963, pp. 21–36.

[5] Donnell, L. H., "New Theory for the Buckling of Thin Cylindrical Shells Under Axial Compression and Bending," *Transactions of the ASME*, Vol. 56, 1934, pp. 795–806.

[6] Ambartsumayan, S. A., "Theory of Anisotropic Shells," TT F-118, May 1964, NASA.

[7] Sobel, L. H., "Effects of Boundary Conditions on the Stability of Cylinders Subject to Lateral and Axial Pressure," *AIAA Journal*, Vol. 2, No. 8, Aug. 1964, pp. 1437–1440.

[8] Forsberg, K., "Influence of Boundary Conditions on the Modal Characteristics of Thin Cylindrical Shells," *AIAA Journal*, Vol. 2, No. 12, Dec. 1964, pp. 2150–2157.

[9] Ralston, A. and Wilf, H. S., *Mathematical Methods for Digital Computers*, Wiley, New York/London, 1960, pp. 95–109.

[10] Hildebrand, F. B., *Introduction to Numerical Analysis*, McGraw-Hill, New York, 1956, pp. 223, 323–325, 345–351.

[11] Norris, C. H. et al., *Structural Design for Dynamic Loads*, McGraw-Hill, New York, 1959, pp. 247, 252.